Research Article Vol. 30, No. 7 / 28 Mar 2022 / Optics Express 10833
Optics EXPRESS

Visible pyramid wavefront sensing approach for daylight adaptive optics

LINSHU HUANG,[1,2] JIANLI WANG,[1,2] LU CHEN,[1] HANGFEI YUAN,[1] HONGZHUANG LI,[1] AND KAINAN YAO[1,*]

[1] *Changchun Institute of Optics, Fine Mechanics and Physics, Chinese Academy of Sciences, Changchun, Jilin 130033, China*
[2] *University of Chinese Academy of Sciences, Beijing 100049, China*
[*] *yaokainan001@126.com*

Abstract: Daytime application of the pyramid wavefront sensor (PyWFS) is greatly challenged by a bright and fluctuating sky background, especially in the visible. A daytime-Py approach to apply visible pyramid wavefront sensing for real-time daylight AO is described in this paper. A field stop (FS) and a lenslet array are applied in the daylight AO system based on a visible PyWFS to separate the object signal from the background signal and improve the signal-to-noise ratio (SNR). A background elimination algorithm is proposed to extract the effective object signal. Closed-loop experiment using the daytime-Py approach is performed, which presents the first laboratory real-time daylight natural guide star AO correction of a faint object based on a visible PyWFS. SNR ranges for both the daytime-Py approach and PyWFS are reported. Furthermore, the correction results in different SNRs using both methods and with various pupil samplings using the daytime-Py approach are presented to prove that our proposal has the advantages over the PyWFS and Shack-Hartmann wavefront sensor (SHWFS) for daylight AO. This study demonstrates that the daytime-Py approach can realize the real-time object tracking and closed-loop correction in the daylight natural guide star adaptive optics (AO) system based on the visible PyWFS.

1. Introduction

The pyramid wavefront sensor (PyWFS) was initially proposed by R. Ragazzoni as a novel phase sensor in 1996. It possesses various advantages such as high sensitivity in closed-loop correction, excellent variable gain characteristics in modulation mode, and adjustable sampling in real-time operation, which makes it a promising alternative for the next-generation astronomical adaptive optics (AO) systems [1–4]. The earliest on-sky correction experiment using PyWFS was performed on AdpOpt@TNG in 1999 [5,6]. Subsequently, PyWFSs have been used to realize wavefront sensing in state-of-the-art AO facilities, such as the Large Binocular Telescope (LBT) [7–9], the Magellan "Clay" telescope [10,11], and Subaru Telescope [12].

The PyWFS is generally used for AO observation during the night. And it has also successfully implemented for ophthalmic applications where the background and read-out noise are higher than the nighttime astronomical AO in the visible [13,14]. However, shot noise induced by the bright daylight background, and the saturation of the wavefront sensor restrict the capabilities of ground-based telescopes used for space situational awareness (SSA) during the day. Additionally, high-resolution observations of resident space objects (RSOs) are severely hampered as many objects of interest will be too faint [15,16]. Despite the limitations of the daytime application of PyWFS, it is an appealing subject, owing to its potential for applications in RSO observation. Successful applications of IR pyramid wavefront sensing have been realized in the facility AO systems. In a previous study, the infrared (IR) PyWFS installed on the Keck II AO bench was applied to obtain the K-band images during the day [17,18]. And Esposito et al. [19] presents the daytime application of the IR PyWFS mounted on the LBT, which is to correct for the

#449021 https://doi.org/10.1364/OE.449021
Journal © 2022 Received 17 Dec 2021; revised 23 Feb 2022; accepted 24 Feb 2022; published 16 Mar 2022

Optics EXPRESS

non-common path aberration (NCPA) between the FLAO system and the LUCI2 N30 IR imager. However, the radiance of the daytime sky background is much brighter in the visible for a given Sun angle than in the IR, because the near blackbody emission of the Sun's radiant energy peaks at the visible wavelengths due to its temperature. The daylight background noise may fluctuate as a function of time and change the light intensity distribution at the PyWFS quickly, which makes the constant threshold algorithm invalid [20,21]. The amount of sky accessible for RSO imaging and the timing of observations are both restricted for the visible PyWFS [22,23]. There have been no studies conducted on real-time daylight natural guide star AO correction based on a visible PyWFS to the best of our knowledge.

Guthery and Hart [24] proposed a hybrid wavefront sensor (HyWFS), which is a significant study for wavefront sensing. The HyWFS combines the non-modulated PyWFS and SHWFS, and captures the ideal features of both the wavefront sensors (WFSs), which is high sensitivity and excellent dynamic range. Our study proposes the implementation of the HyWFS in the daylight AO system. Except for the original features of HyWFS, the new structure brings other attractive properties for daylight AO.

This paper presents a daytime-Py approach to realize real-time daylight pyramid wavefront sensing in the visible. A field stop (FS) is employed to block the extended background light, and a lenslet array is used to distinguish the object signal from the sky background signal and improve the signal-to-noise ratio (SNR). A background elimination algorithm is proposed to extract the clear object information. In the following sections, the principle and algorithm of the daytime-Py approach are introduced and experimentally demonstrated in a daylight AO system. The daylight AO correction results using this approach and visible PyWFS alone are reported and compared, indicating that our approach provides stable and accurate real-time daylight correction while the PyWFS does not. Furthermore, the correction results in the different SNRs using both methods and the SNR ranges applicable for both methods are reported. The daylight AO corrections with different pupil samplings using the daytime-Py approach are presented. Our approach provides adjustable pupil sampling in real time and higher sensitivity for daylight AO when compared to the visible SHWFS. The daytime-Py approach can be used to realize the real-time daytime application of the visible PyWFS and it is proved experimentally to be an alternative for daylight natural guide star AO correction in the visible.

2. Daytime-PyWFS for daylight AO

2.1. Daytime-PyWFS principle for daylight AO

Figure 1 presents the schematic diagram of the PyWFS. The incident beam is focused on the tip of the pyramid by focusing lens1 (L1) and is then divided into four separate beams. Four subpupil images are generated on the detector through relay lens2 (L2).

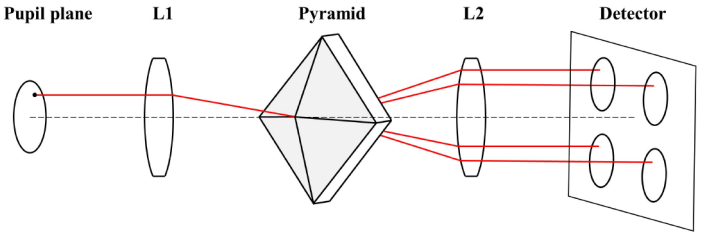

Fig. 1. Schematic diagram of a PyWFS.

However, the relatively strong daylight sky background signal in the daytime obscures the weak object signal in the PyWFS output images, which results in the low SNR detected by the PyWFS. A lenslet array is added to the daylight AO system based on the PyWFS to improve the

Optics EXPRESS

detection capability of the PyWFS for daylight AO. Figure 2 presents the schematic diagram of the daytime-PyWFS (a double pyramid is used here) during the daytime. The object light is represented by the red line, while the gray area represents the sky background light. An FS is placed before the pyramid prism and its size can be adjusted to ensure that the background signal in each subaperture is low and does not overlap. The sky background light is an extended disk on the tip of the pyramid prism, and the object light is focused into a point located at the center of the disk when passing through the FS. A lenslet array is then placed at the PyWFS pupil plane to separate the object signal from the sky background signal in the PyWFS output subpupil images. The lens2 (L2) and lenslet form a 4f system, thus the pyramid prism vertex plane and the sCMOS detection plane are conjugated. As a result, the background light is imaged as four quarter-circle arrays, while the object light is imaged as four spot arrays on the detector, as shown in Figs. 2(b) and 2(c).

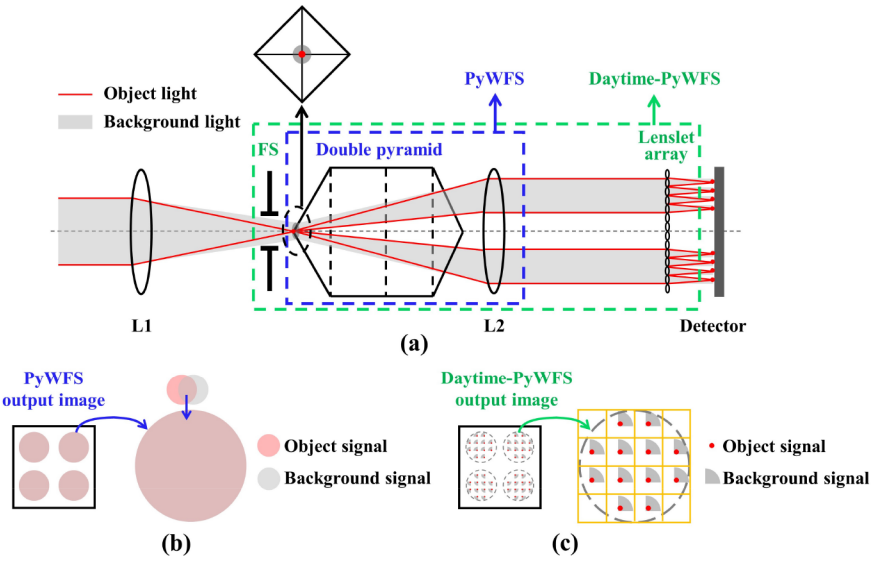

Fig. 2. (a)Schematic diagram of the daytime-PyWFS during the daytime. The blue dotted box indicates the PyWFS optical layout, and the green box indicates the daytime-PyWFS optical layout. (b) The PyWFS output image with the object signal and background signal. (c) The daytime-PyWFS output image with the object signal and background signal. Each area divided by the yellow solid lines represents a subaperture.

The object signal is separated from the background signal. In the same manner as the PyWFS output signals, the daytime-PyWFS output signals are calculated as the gradient of the object wavefront:

$$S_x(i,j) = \frac{I_1(i,j) - I_2(i,j) - I_3(i,j) + I_4(i,j)}{I_1(i,j) + I_2(i,j) + I_3(i,j) + I_4(i,j)} \tag{1}$$

$$S_y(i,j) = \frac{I_1(i,j) + I_2(i,j) - I_3(i,j) - I_4(i,j)}{I_1(i,j) + I_2(i,j) + I_3(i,j) + I_4(i,j)} \tag{2}$$

where $I_1(i,j) \sim I_4(i,j)$ represent the object signal in the subaperture (i,j) of the subpupil image 1~4, separately.

2.2. Performance analysis

High-resolution daytime imaging of RSOs from the ground is challenging as one cannot collect enough light from the object to achieve adequate SNR in the presence of high daylight background

Optics EXPRESS

noise [22]. SNR is a critical index for the detection capability of a practical AO system [3], and it is defined as the ratio of the object intensity to the background intensity:

$$SNR = \frac{S}{\sqrt{N_{object}^2 + N_{background}^2 + N_{read}^2 + N_{dark}^2}} \tag{3}$$

where S represents the object intensity. N_{object}^2 and $N_{background}^2$ represent the photon noise introduced by object and background separately. N_{read}^2 represents the read-out noise, and N_{dark}^2 represents the dark current noise. To realize the successful daylight closed-loop AO correction, the adequate SNR detected by the WFS is necessary and it means the WFS has a great detection capability. The object signal needs to be strong enough for real-time extraction, otherwise it would be blurred by the high daylight background noise. The object noise N_{object}^2 can be neglected as the object is much fainter than the daylight background, and the dark current noise N_{dark}^2 is also very small due to the short exposure time. Shot noise introduced by the bright sky background becomes the main noise source and causes a sharp detection capability decline of WFSs. For daylight AO, Eq. (3) can be written as:

$$SNR = \frac{S}{\sqrt{N_{background}^2 + N_{read}^2}} \tag{4}$$

The object intensity in SNR is defined as the average photon count of the object pixels, and the background intensity is described as the standard deviation of the photons of the background pixels. For the usual PyWFS, the object photons are distributed throughout the PyWFS subpupil images and buried by the relatively strong and fluctuating daylight background noise. The distribution of background values fits the Gaussian probability density function (PDF) in the time domain, and the PDF is expressed as [21]:

$$\eta(\nu_t, \mu_t, \sigma_t) = \frac{1}{\sqrt{2\pi}\sigma_t} e^{\frac{-(\nu_t - \mu_t)^2}{2{\sigma_t}^2}} \tag{5}$$

where ν_t is the pixel value at time t. μ_t and σ_t are the mean value and standard variance of the Gaussian distribution at time t. It can be observed that the background photon noise fluctuates at the mean pixel value as a function of time. The constant threshold algorithm is invalid for the PyWFS, as the large fluctuation of background photon noise makes the SNR still be extremely low. For the SHWFS, it has a superior detection capability than the PyWFS, as the object photons are concentrated and the background noise is even. However, the SHWFS suffers from the noise propagation and produces estimation errors [25], which means high-order wavefront errors cannot be corrected effectively at the same time as low-order terms. For the daytime-PyWFS, the object photons are greatly concentrated while the daylight background noise is relatively uniform in each subaperture. The object photon count detected by the daytime-PyWFS are much higher than that detected by the PyWFS, which makes the SNR increase. It has the similar detection capability to the SHWFS in the open loop. However, the daytime-PyWFS uses the slope signal computed from four subpupil images (as seen in Eqs. (1) and (2)) as the input for wavefront control, so it can offer the diffraction limit of full aperture in the closed loop [24]. Moreover, the daytime-PyWFS offers real-time adjustable pupil sampling in closed-loop correction, while the SHWFS cannot.

3. Daylight AO system based on the visible daytime-PyWFS

3.1. Optical layout and imaging experimental results

High-resolution observation is more challenging at visible wavelengths than at IR wavelengths during the daytime. A daylight AO system based on the daytime-PyWFS is established to

Optics EXPRESS

determine the feasibility of the daytime-PyWFS for daylight AO. Figure 3 presents the optical layout of the daylight AO system, and Fig. 4 presents the relevant photographs. A fiber-coupled laser source with a wavelength of 660 nm is used to simulate weak object light and an LED surface light source is used to simulate strong sky background light in the visible band. Three optical attenuators are placed after the laser source as the laser intensity is too high for the CCD camera to measure the signals or provide images. The background light is reflected by beam-splitter1 (BS1) and converges with the weakened object light to form the incident light. The mixed light is reflected by a deformable mirror (DM) and focused by lens2 (L2). The beam-splitter3 (BS3) splits the incident light into two beams. One beam is focused on the CCD camera. The other passes through field stop2 (FS2) and is split into four subbeams by the double pyramid. The subbeams are then focused by the lenslet array and imaged on the sCMOS camera.

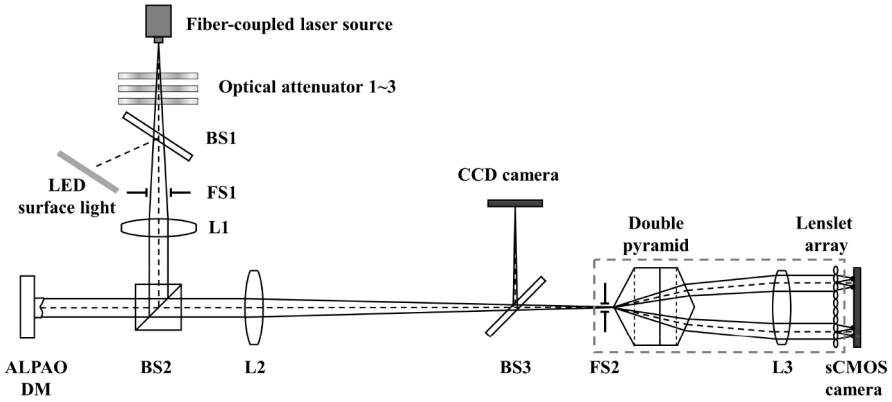

Fig. 3. Optical setup of the daylight AO system based on the daytime-PyWFS. The area outlined by the gray dotted line represents daytime-PyWFS.

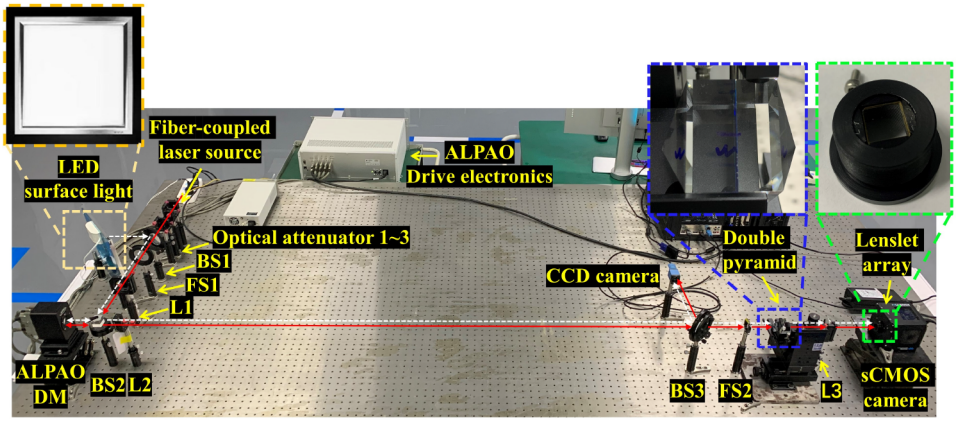

Fig. 4. Photograph of the daylight AO system laboratory setup based on the daytime-PyWFS.

The DM used in this study is ALPAO DM192, which is a 192-element continuous reflective surface DM. A double pyramid is used instead of a single pyramid for the PyWFS, as shown in Fig. 5. It is easier to manufacture because of its much higher base angles, and the chromatic aberration introduced by a single pyramid can be reduced [26]. The sCMOS camera is Kinetix Scientific CMOS Camera made by Teledyne Photometrics and the CCD camera is DMK

Optics EXPRESS

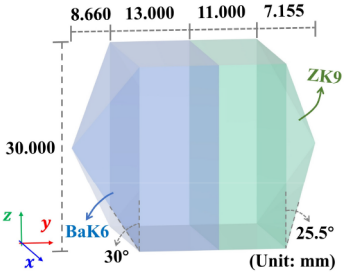

Fig. 5. Schematic of the double pyramid used in the experiment.

Table 1. Parameters of the daylight AO experiment

Device	Parameter	Value
Laser source	Wavelength of the laser source	660 nm
LED source	Power of LED source	10 W
Lens	L1 focal length	500 mm
	L2 focal length	2000 mm
	L3 focal length	150 mm
DM	Number of actuators	192 (16 × 16 distribution)
	Pitch	1.5 mm
	Pupil diameter	21 mm
	Tip/tilt stroke	15μm
Lenslet array	Lenslet side lengths	0.2mm × 0.2mm
	Lenslet focal length	7.0 mm
	Number of lenslets	50 × 50
	Number of effective lenslets in subpupil images	52 (8 × 8 distribution)
sCMOS camera	Pixel area	6.5μm × 6.5μm
	Sensor area	20.8mm × 20.8mm
	Peak quantum efficiency (QE)	> 95% at 600 nm
	Bit-depth	16-bit
	Read noise	16 e-
CCD camera	Pixel area	3.75μm × 3.75μm
	Sensor area	4.8mm × 3.6mm
	Peak quantum efficiency (QE)	> 70% at 520 nm
	Bit-depth	8-bit

23UM021 made by The Imaging Source. Table 1 lists more specific parameters of the daylight AO experiment.

The function of the lenslet array is verified by contrasting the output images of the PyWFS and daytime-PyWFS in the daylight AO system. The FS2 placed before the pyramid prism is not moved in this experiment. Figure 6 depicts the PyWFS output images of different incident lights. The pure object signal is much weaker than the background signal, as shown in Figs. 6(a) and 6(b). In the simulated daytime condition when the object light and background light are mixed as the incident light, the PyWFS output image is shown in Fig. 6(c). In the daytime, the object signal is blurred by the relatively strong background signal, especially in the visible. It is

Optics EXPRESS

almost impossible for the visible PyWFS alone to provide any effective object information in real time for daylight AO due to the varying daylight.

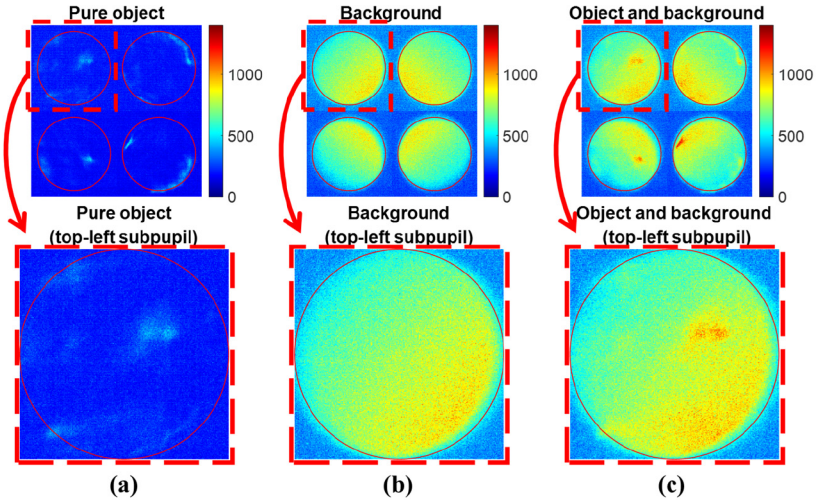

Fig. 6. Output images of the visible PyWFS in the daylight AO system: (a) the image with the pure object light; (b) the image with the background light; (c) the image with the object and the background light.

Figure 7 illustrates the daytime-PyWFS output images of various incident lights. Each subbeam passes through 8×8 lenslets. The object photons are collected through the lenslet array, and the output image of the pure object light has four spot array patterns, as shown in Fig. 7(a). The output image of the background light has four quarter-circle array patterns, as shown in Fig. 7(b). When the object light and background light are mixed to form the incident light, the daytime-PyWFS output image is presented in Fig. 7(c). The results indicate that the lenslet array can be used to distinguish the object signal from the background signal in the PyWFS subpupil images for daylight AO.

3.2. SNR improvement

The SNRs detected by the PyWFS and daytime-PyWFS are calculated to demonstrate that the daytime-PyWFS has a better detection capability for real-time wavefront sensing in the daylight AO system. Four subpupil images are summed to obtain the complete information of the incident light for both the WFSs. With 8×8 pupil sampling, SNR_{WFS} is calculated as the mean SNR in the 52 effective subapertures with the mixed incident light, and is expressed by:

$$SNR_{WFS} = \frac{\sum_{j=1}^{N_l} \sum_{i=1}^{N_l} SNR_{aperture}(i,j)}{N_{aperture}} \tag{6}$$

where $\left(i - \frac{N_l}{2}\right)^2 + \left(j - \frac{N_l}{2}\right)^2 \leq \left(\frac{N_l}{2}\right)^2$. N_l represents the number of subapertures across the diameter of each subpupil image, and $N_{aperture}$ represents the number of effective subapertures in the subpupil image. $SNR_{aperture}(i,j)$ represents the SNR detected by the WFS in the subaperture (i,j) and is expressed by Eq. (7). As indicated in section 2.2, the object intensity $S_{object}(i,j)$ is the average photon count of the object pixels in subaperture (i,j), and the background intensity is

Optics EXPRESS

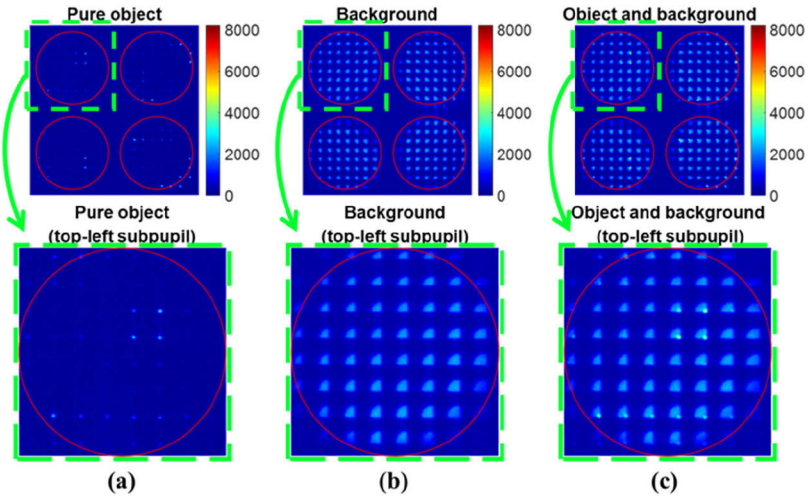

Fig. 7. Output images of the visible daytime-PyWFS in the daylight AO system: (a) the image with the pure object light; (b) the image with the background light; (c) the image with the object light and background light.

described as the standard deviation of the background and read-out noise pixel values.

$$SNR_{aperture}(i,j) = \frac{S_{object}(i,j)}{\sqrt{N^2{}_{background} + N^2{}_{read}}} \tag{7}$$

For the PyWFS, the object photons are distributed throughout the subpupil images, so $S_{object}(i,j)$ is described by the mean pixel value in the subaperture (i,j). 2000 consecutive PyWFS images with the object signal are collected, and $S_{object}(i,j)$ is calculated as the mean value of the 2000 data elements in subaperture (i,j). The background intensity is calculated as the standard deviation of all the background pixel values in the PyWFS pupil image. According to Eqs. (6) and (7), SNR_{PyWFS} is calculated to be 0.3.

For the daytime-PyWFS, the object photons are greatly concentrated in only several pixels in each subaperture. The object pixel values are similar and much larger than the rest background pixel values. To simplify the calculation, the peak object pixel value in the spot area of the subaperture (i,j) can be utilized to express $S_{object}(i,j)$ since it is very close to the mean object pixel value. A total of 2000 consecutive daytime-PyWFS images with the object signal are captured, and the mean value of the 2000 data elements in the subaperture (i,j) is used to express $S_{object}(i,j)$. The background intensity is described by the standard deviation of all the background pixel values in the quarter-circle area of the daytime-PyWFS pupil image. As a result, $SNR_{daytime-PyWFS}$ is calculated to be 4.3 with the same incident object and background light. Based on the contrast of the SNR, it can be concluded that the detection capability of the visible PyWFS for daylight AO is greatly enhanced with the help of the lenslet array.

4. Background elimination algorithm

The object signal is separated from the background signal in the daytime-PyWFS output image. And a background elimination algorithm is proposed to extract the object intensity information. In our experiment, each subpupil image occupies 240×240 pixels, and each subaperture occupies 30×30 pixels with 8×8 pupil sampling, as shown in Fig. 8(a). The effective information of the object light and background light is only included in the quarter-circle area of the subaperture.

Optics EXPRESS

The background elimination algorithm for the daytime-PyWFS is explained as follows: (1) the quarter-circle area with a radius of approximately 14 pixels is first extracted in each subaperture and the maximum value is located; (2) approximately 5×5 pixels around the coordinates are eliminated, as shown in Fig. 8(b); (3) the background intensity distribution $B_{i,j}$ is obtained by calculating the mean value and standard deviation of the pixel values in the remaining area of the subaperture (i, j), as shown in Fig. 8(c); (4) the daylight intensity $B_{i,j}$ is subtracted from the pixel values $I_{i,j}(x, y)$ whose coordinate is (x, y) in the subaperture (i, j). The pixel value after the background subtraction $I_{i,j}'(x, y)$ can be expressed as Eq. (8). As a result, the experimental result

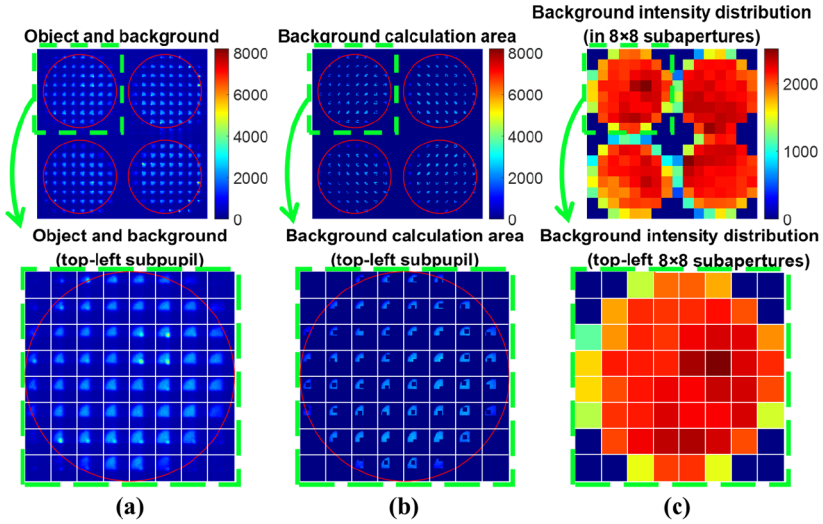

Fig. 8. Process of the background elimination algorithm. Each area divided by the white line represents a subaperture. (a) Initial daytime-PyWFS output image with the mixed signal, (b) background calculation areas in the subapertures of daytime-PyWFS output image, and (c) background intensity distribution (unit: subaperture) of daytime-PyWFS output image.

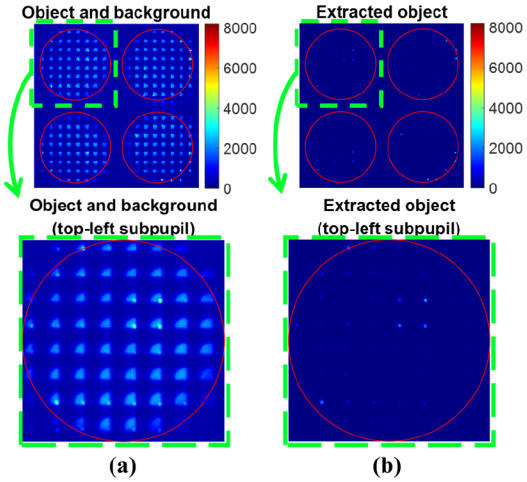

Fig. 9. Experimental results of the background elimination algorithm: (a) Initial daytime-PyWFS output image with the mixed signal, and (b) the object information extracted by the background elimination algorithm.

Optics EXPRESS

of the background elimination algorithm is presented in Fig. 9. It is shown that the main object information in the daytime-PyWFS output image is extracted effectively.

$$I_{i,j}{}'(x,y) = \begin{cases} 0 & I_{i,j}(x,y) \le B_{i,j} \\ I_{i,j}(x,y) - B_{i,j} & I_{i,j}(x,y) > B_{i,j} \end{cases} \tag{8}$$

The background elimination algorithm determines the background intensity to the subaperture accuracy, so it has better precision compared with the traditional constant threshold algorithm. And it is more suitable for real-time operation compared with the correlation algorithm considering about the computational cost [27].

5. Closed-loop daylight experiment based on the daytime-Py approach

The daytime-Py approach is proposed based on the daytime-PyWFS and the background elimination algorithm. The main advantage of our proposal over the usual PyWFS is that it enables real-time wavefront sensing at the visible wavelengths in the daylight AO system. Closed-loop daylight AO correction experiments are carried out to demonstrate the performance of the daytime-Py approach and PyWFS in the conditions where the daylight background changes quickly.

5.1. Closed-loop daylight AO correction results

The daylight AO experimental setup is shown in Fig. 4. A data binning operation is performed in the process of slope signal calculation. Each group of 30×30 pixels is binned to a single pixel for each subaperture with 8×8 pupil sampling, ensuring precision and simultaneously simplifying the computation process. The DM is applied to introduce the initial wavefront distortion and to achieve fast and accurate wavefront corrections. The Zernike order used is the Noll ordering without the piston mode [28].

The daylight AO system is calibrated with only the object light before closing the loop. The WFS responses to the Zernike modes applied to the DM are measured by Eqs. (1) and (2) and give the columns of the interaction matrix. The calibration matrix is then obtained by inverting the interaction matrix using a standard single-value decomposition algorithm. The main difference in the calibration between the two methods is that the read-out noise is eliminated in the daytime-Py approach case using the background elimination algorithm, since the background pixel values are set to zero in the correction. However, the background subtraction is not utilized for the usual PyWFS. The daylight background varies quickly, making it almost impossible to be determined in real-time daylight object tracking and correction. In the closed-loop AO correction experiment, the object light mixes with the background light as the incident light. The static wavefront distortion is deliberately introduced by the DM and aberrates the object light. In the daytime-PyWFS case, the object information is extracted by the background elimination algorithm and then used for WFS signals calculation. With the WFS response and calibration matrix, a set of Zernike coefficients is obtained in each iteration for wavefront compensation.

The daylight AO closed-loop corrections are performed using the daytime-Py approach and PyWFS when the SNR is 4.3 (calculated by Eqs. (6) and (7)), and the experimental results with an initial RMS of 1.109λ are presented Fig. 10. The incident wavefront distortion is formed by Z4(0.7λ), Z5(0.6λ), Z6(0.3λ), Z8(0.2λ), and Z9(0.5λ). Figures 10(a) and 10(b) present the original wavefront image and the focal plane image before the correction. After the correction using the daytime-Py approach, the wavefront distortion is eliminated and the focal plane spot energy is notably concentrated, as shown in Figs. 10(c) and 10(d). And RMS of the remaining wavefront is approximately 0.044λ after 50 iterations, as shown in Fig. 10(e). However, the closed-loop correction experiment using the usual PyWFS has to be terminated after 20 iterations to prevent

Optics EXPRESS

damage to the DM. The quality of the image deteriorates rapidly and the remaining wavefront RMS value continues to increase, as shown from Figs. 10(f) to 10(h). The results indicate that the daytime-Py approach provides stable real-time daylight closed-loop AO correction, while the usual PyWFS is impractical.

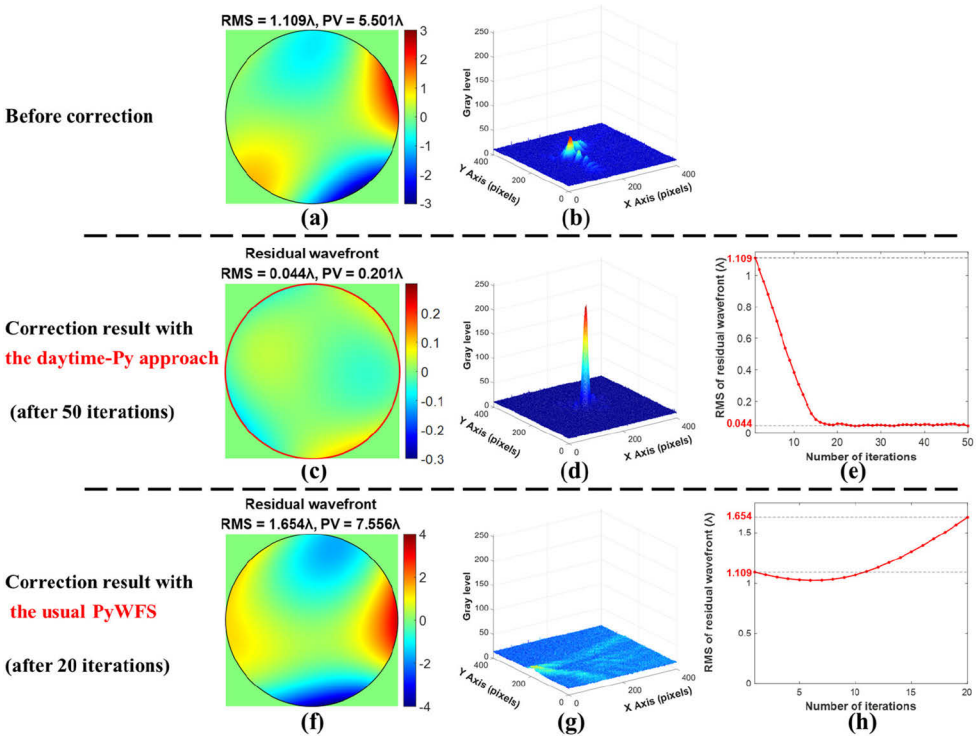

Fig. 10. Correction results using the two methods. Before correction, (a) the wavefront image and (b) focal plane image. Correction results using the daytime-Py approach: (c) the wavefront image, (d) the focal plane image, and (e) plot of residual wavefront RMS as a function of iterations. Correction results using the usual PyWFS: (f) the wavefront image, (g) the focal plane image, and (h) plot of residual wavefront RMS as a function of iterations.

Another static wavefront aberration with an initial RMS of 1.122λ is introduced to increase the credibility of the experiment. The incident wavefront distortion is formed by Z4(0.8λ), Z5(0.5λ), Z6(0.1λ), and Z8(0.6λ). Figures 11–13 present the correction results obtained by using the daytime-Py approach. The quality of the image is significantly improved, as shown in Fig. 11 and Fig. 12. The RMS of the residual wavefront decreases from 1.122λ to 0.041λ, as shown in Fig. 13(a). The variation of the Strehl ratio (relative to the final frame), which represents the quality of the image in the focal plane camera, is improved by the proposed method, as seen in Fig. 13(b).

5.2. SNR range

The SNR ranges for both the daytime-Py approach and usual PyWFS are obtained experimentally. For ease of illustration and comparison, it should be noted that the following SNRs are calculated using Eqs. (6) and (7) based on the daytime-PyWFS structure. Real-time daylight closed-loop corrections with three different static wavefront aberrations are performed in each SNR condition to increase the accuracy of the result. The criterion for successful correction is that the remaining wavefront RMS values with the three wavefront aberrations is less than 0.100λ when the system is

Optics EXPRESS

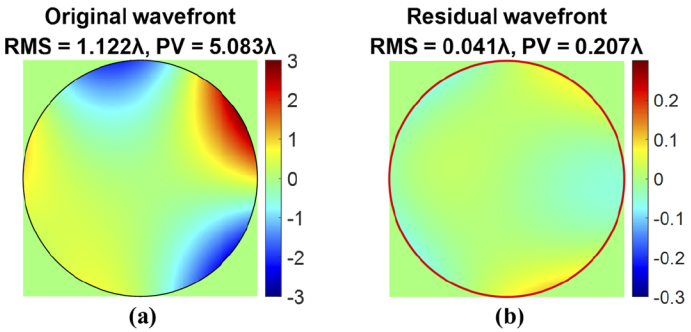

Fig. 11. The wavefront images: (a) the original wavefront image with an RMS of 1.122λ, and (b) the residual wavefront image with an RMS of 0.041λ after closed-loop correction using the daytime-Py approach.

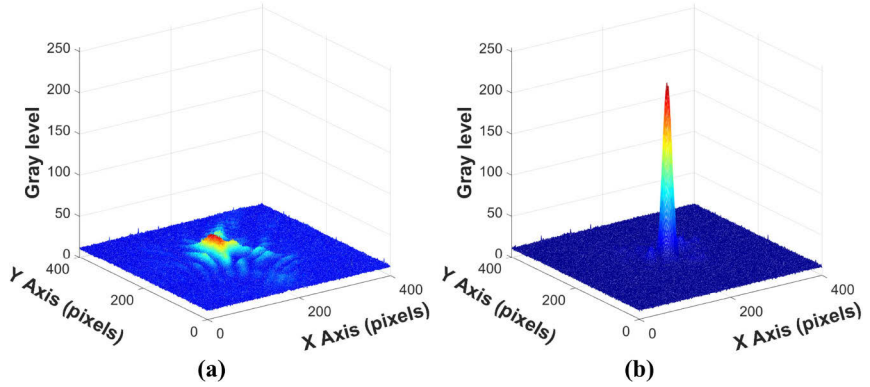

Fig. 12. The focal plane images: (a) the original focal plane image, and (b) the focal plane image after closed-loop correction using the daytime-Py approach.

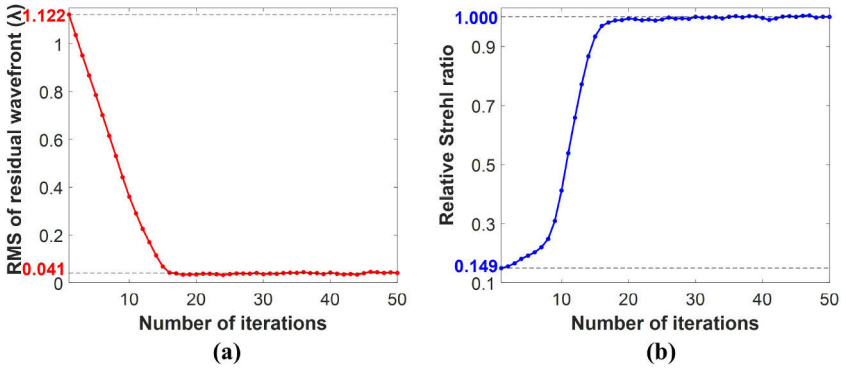

Fig. 13. (a) Plot of residual wavefront RMS as a function of iterations, and (b) relative SR as a function of iterations using the daytime-Py approach.

Optics EXPRESS

stable. Apart from the wavefront aberrations with an initial RMS of 1.109λ and 1.122λ mentioned above, another one with an initial RMS of 1.166λ is formed by Z4(0.5λ), Z5(0.7λ), Z6(0.2λ), Z8(0.7λ), and Z9(0.3λ). The SNR is changed by adjusting the incident object light intensity, until the minimum SNR for the method to correct the wavefront aberrations successfully is found.

As a result, the daytime-Py approach is proved to be available for daylight AO closed-loop correction when the SNR is greater than 1.9. The correction results using the daytime-Py approach when the SNR is 1.9 and 4.3 are compared, as shown in Fig. 14. Referring to the initial RMS of 1.166λ, the remaining RMS is 0.075λ when SNR is 1.9, and it is 0.042λ when SNR is 4.3. The correction result is better when SNR is 4.3.

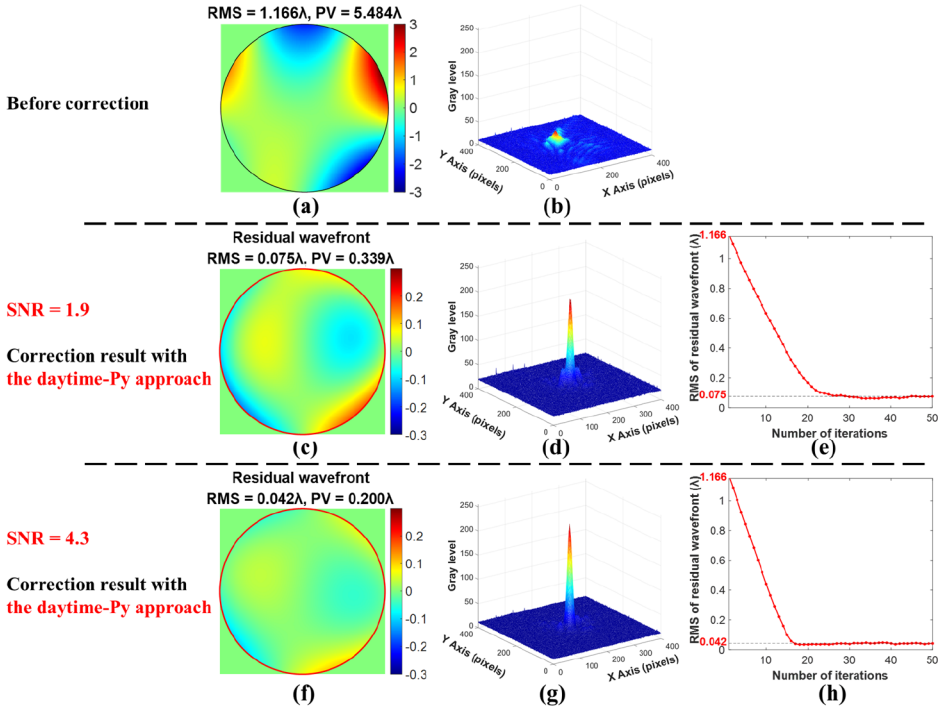

Fig. 14. Correction results for different SNRs using the daytime-Py approach. Before correction, (a) the wavefront image and (b) focal plane image. Correction results when SNR is 1.9: (c) the wavefront image, (d) the focal plane image, and (e) plot of residual wavefront RMS as a function of iterations. Correction results when SNR is 4.3, (f) the wavefront image, (g) the focal plane image, and (h) plot of residual wavefront RMS as a function of iterations.

Furthermore, the usual PyWFS is proved to be available for real-time daylight closed-loop correction when the SNR is greater than 16.9. The correction results when SNR is 16.9 using both the methods are presented in Fig. 15. It can be seen that both the usual PyWFS and daytime-Py approach achieve the successful correction. However, the daytime-Py approach eliminates the wavefront aberration more effectively and makes the focal plane energy more concentrated after correction. More closed-loop experimental results in different SNRs using both the methods are presented in Table 2.

To summarise, neither of the two approaches is practical when SNR is less than 1.9. Only the daytime-Py approach is practical when SNR is larger than 1.9 but less than 16.9. Both techniques are viable when SNR is larger than 16.9. Furthermore, the daytime-Py approach outperforms the

Optics EXPRESS

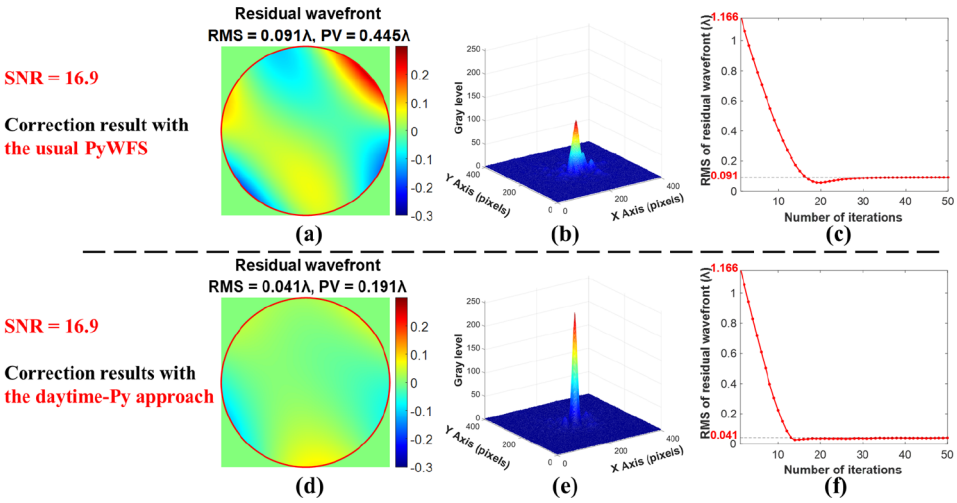

Fig. 15. Correction results when SNR is 16.9 using both the methods. Correction results with the usual PyWFS: (a) the wavefront image, (b) the focal plane image, and (c) plot of residual wavefront RMS as a function of iterations. Correction results with the daytime-Py approach: (d) the wavefront image, (e) the focal plane image, and (f) plot of residual wavefront RMS as a function of iterations.

Table 2. In different SNRs, daylight AO correction results using the daytime-Py approach and PyWFS

SNR	Initial RMS	Daytime-Py approach		PyWFS	
		Final RMS (After 50 iterations)	Iteration times for system stability	Final RMS (After 50 iterations)	Iteration times for system stability
1.9	1.109λ	0.086λ	26	×[a]	×
	1.122λ	0.049λ	28	×	×
	1.166λ	0.075λ	29	×	×
4.3	1.109λ	0.041λ	17	×	×
	1.122λ	0.040λ	15	×	×
	1.166λ	0.041λ	16	×	×
16.9	1.109λ	0.039λ	10	0.091λ	19
	1.122λ	0.037λ	11	0.091λ	16
	1.166λ	0.041λ	13	0.091λ	16

[a]The distorted wavefront cannot be corrected.

Optics EXPRESS

usual PyWFS in real-time daylight closed-loop AO corrections since it can operate in lower SNR and realize better correction results in the same SNR.

5.3. Pupil sampling

The daytime-Py approach allows for real-time adjustable sampling to achieve the optimum system performance. Low sampling is appropriate for faint objects and improves sensing speed, but it can also reduce sensing accuracy. The closed-loop correction results with pupil sampling of 4×4 and 8×8 are presented in Fig. 16. The initial RMS of the wavefront is 1.166λ. With 4×4 pupil sampling, the residual wavefront RMS is 0.084λ and the system tends to stabilize after 11 iterations. With 8×8 pupil sampling, the residual wavefront RMS is 0.042λ and the system tends to stabilize after 16 iterations. Table 3 presents more daylight AO correction experimental results with different pupil samplings using this approach.

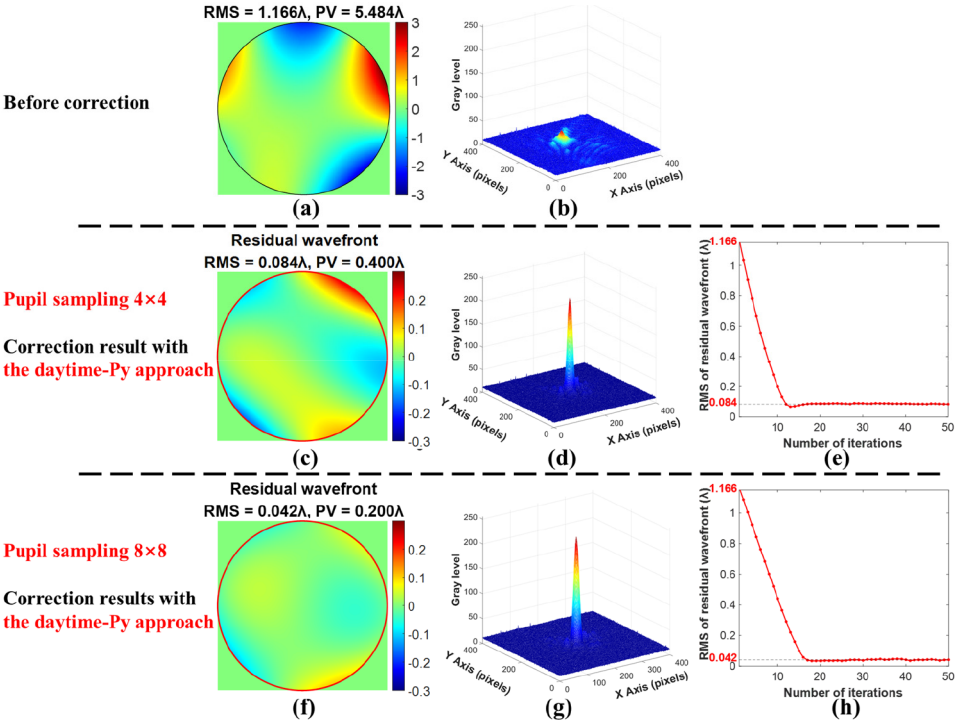

Fig. 16. Correction results with different pupil samplings using the daytime-Py approach. Before correction, (a) the wavefront image and (b) focal plane image. Correction results with 4×4 pupil sampling: (c) the wavefront image, (d) the focal plane image, and (e) plot of residual wavefront RMS as a function of iterations. Correction results with 8×8 pupil sampling: (f) the wavefront image, (g) the focal plane image, and (h) plot of residual wavefront RMS as a function of iterations.

The daylight AO correction results with different pupil samplings using the daytime-Py approach demonstrate that this approach can be used with adjustable pupil sampling in real-time operation, which is better than the SHWFS for daylight AO.

Optics EXPRESS

Table 3. With different pupil samplings, daylight AO correction results using the daytime-Py approach

Pupil sampling	Initial RMS	Final RMS (after 50 iterations)	Iteration times for system stability
4×4	1.109λ	0.087λ	10
	1.122λ	0.087λ	10
	1.166λ	0.084λ	11
8×8	1.109λ	0.044λ	17
	1.122λ	0.041λ	15
	1.166λ	0.042λ	16

6. Conclusion

This paper theoretically and experimentally presents an approach to visible pyramid wavefront sensing for real-time daylight natural guide star AO closed-loop corrections. The daytime-PyWFS is used to differentiate object signal from the background signal preliminary and improve SNR. The background elimination algorithm is then used to extract the pure object signal. The closed-loop AO correction is performed using the daytime-Py approach, which presents the first publicly reported laboratory real-time daylight AO correction result based on a visible PyWFS. For the incident wavefront distortion with an initial RMS of 1.109λ, the correction results for both the daytime-Py approach and usual PyWFS are contrasted, showing that the daytime-Py approach can be used for real-time daylight AO correction in low SNR, while the usual PyWFS is impracticable. The correction results for the daytime-Py approach with an initial RMS of 1.122λ are presented to further verify the feasibility of this approach. Furthermore, the SNR ranges for both the methods are presented. The daytime-Py approach is available for real-time daylight AO correction when the SNR is greater than 1.9, and the usual PyWFS is available when the SNR is greater than 16.9. And the correction results in different SNRs using both the methods and with different pupil samplings using the daytime-Py approach are presented. To summarise, our proposal has better performance in the real-time daylight AO closed-loop corrections in low SNR compared with the usual PyWFS. And it presents higher sensitivity and adjustable pupil sampling in real time for daylight AO compared with the SHWFS. The proposed approach enables high-resolution observation of RSOs during both daytime and nighttime, and also allows for the daylight natural guide star AO tracking and correction of solar-illuminated object. Moreover, the daytime-Py approach is expected to be performed in the field experiment on the 4.0 m telescope which we are working on.

Funding. Chinese Academy of Sciences Key Project (YZQT024).

Disclosures. The authors declare no conflicts of interest.

Data availability. Data underlying the results presented in this paper are not publicly available at this time but may be obtained from the authors upon reasonable request.

References

1. R. Ragazzoni, "Pupil plane wavefront sensing with an oscillating prism," J. Mod. Opt. **43**(2), 289–293 (1996).
2. R. Ragazzoni and J. Farinato, "Sensitivity of a pyramidic Wave Front sensor in closed loop Adaptive Optics," Astron. Astrophys. **350**(2), 23–26 (1999).
3. K. Yao, J. Wang, X. Liu, H. Li, M. Wang, B. Cui, and S. Yu, "Pyramid wavefront sensor using a sequential operation method," Appl. Opt. **54**(13), 3894–3901 (2015).
4. L. Chen, J. Wang, K. Yao, X. Liu, X. Lin, L. Wang, and M. Wang, "Experimental Demonstration of Sequential Operation Approach for a Three-Sided Pyramid Wavefront Sensor," IEEE Photonics J. **8**(4), 1–13 (2016).
5. R. Ragazzoni, A. Baruffolo, J. Farinato, A. Ghedina, E. Marchetti, S. Esposito, L. Fini, P. Ranfagni, F. Bortoletto, M. D'Alessandro, M. Ghigo, and G. Crimi, "The final commissioning phase of the AdOpt@TNG module," in *Adaptive Optical Systems Technology*, (2000), pp. 57–62.
6. R. Ragazzoni, A. Ghedina, A. Baruffolo, E. Marchetti, J. Farinato, T. Niero, G. Crimi, and M. Ghigo, "Testing the pyramid wavefront sensor on the sky," in *Adaptive Optical Systems Technology*, (2000), pp. 423–430.

Optics EXPRESS

7. S. Esposito, A. Riccardi, F. Quirós-Pacheco, E. Pinna, A. Puglisi, M. Xompero, R. Briguglio, L. Busoni, L. Fini, P. Stefanini, G. Brusa, A. Tozzi, P. Ranfagni, F. Pieralli, J. C. Guerra, C. Arcidiacono, and P. Salinari, "Laboratory characterization and performance of the high-order adaptive optics system for the Large Binocular Telescope," Appl. Opt. **49**(31), G174 (2010).
8. S. Esposito, A. Riccardi, E. Pinna, A. Puglisi, F. Quirós-Pacheco, C. Arcidiacono, M. Xompero, R. Briguglio, G. Agapito, L. Busoni, L. Fini, J. Argomedo, A. Gherardi, G. Brusa, D. Miller, J. C. Guerra, P. Stefanini, and P. Salinari, "Large Binocular Telescope Adaptive Optics System: New achievements and perspectives in adaptive optics," in *Astronomical Adaptive Optics Systems and Applications IV*, (2011).
9. S. Esposito, A. Riccardi, E. Pinna, A. T. Puglisi, F. Quirós-Pacheco, C. Arcidiacono, M. Xompero, R. Briguglio, L. Busoni, L. Fini, J. Argomedo, A. Gherardi, G. Agapito, G. Brusa, D. L. Miller, J. C. Guerra Ramon, K. Boutsia, and P. Stefanini, "Natural guide star adaptive optics systems at LBT: FLAO commissioning and science operations status," in *Adaptive Optics Systems III*, (2012), pp. 84470U–84411.
10. D. Kopon, L. M. Close, J. R. Males, and V. Gasho, "Design, implementation, and on-sky performance of an advanced apochromatic triplet atmospheric dispersion corrector for the Magellan adaptive optics system and VisAO camera," Publ. Astron. Soc. Pac. **125**(930), 966–975 (2013).
11. K. M. Morzinski, L. M. Close, J. R. Males, D. Kopon, P. M. Hinz, S. Esposito, A. Riccardi, A. Puglisi, E. Pinna, R. Briguglio, M. Xompero, F. Quirós-Pacheco, V. Bailey, K. B. Follette, T. J. Rodigas, Y.-L. Wu, C. Arcidiacono, J. Argomedo, L. Busoni, T. Hare, A. Uomoto, and A. Weinberger, "MagAO: Status and on-sky performance of the Magellan adaptive optics system,"in *Adaptive Optics Systems IV*, (2014).
12. N. Jovanovic, F. Martinache, O. Guyon, C. Clergeon, G. Singh, T. Kudo, V. Garrel, K. Newman, D. Doughty, J. Lozi, J. Males, Y. Minowa, Y. Hayano, N. Takato, J. Morino, J. Kuhn, E. Serabyn, B. Norris, P. Tuthill, G. Schworer, P. Stewart, L. Close, E. Huby, G. Perrin, S. Lacour, L. Gauchet, S. Vievard, N. Murakami, F. Oshiyama, N. Baba, T. Matsuo, J. Nishikawa, M. Tamura, O. Lai, F. Marchis, G. Duchene, T. Kotani, and J. Woillez, "The Subaru Coronagraphic Extreme Adaptive Optics System: Enabling High-Contrast Imaging on Solar-System Scales," Publ. Astron. Soc. Pac. **127**(955), 890–910 (2015).
13. S. R. Chamot, C. Dainty, and S. Esposito, "Adaptive optics for ophthalmic applications using a pyramid wavefront sensor," Opt. Express **14**(2), 518–526 (2006).
14. E. M. Daly and C. Dainty, "Ophthalmic wavefront measurements using a versatile pyramid sensor," Appl. Opt. **49**(31), G67–G77 (2010).
15. M. Hart, "Image registration for daylight adaptive optics," Opt. Lett. **43**(6), 1391–1394 (2018).
16. M. Hart, D. A. Hope, J. Richey, and T. R. Swindle, "Image Restoration from Sodium Guide Star Observations in Daylight," in *Advanced Maui Optical and Space Surveillance Technologies Conference*, (2019).
17. C. Z. Bond, P. Wizinowich, M. Chun, D. Mawet, S. Lilley, S. Cetre, N. Jovanovic, J. Delorme, E. Wetherell, S. Jacobson, C. Lockhart, E. Warmbier, J. Wallace, D. Hall, S. Goebel, O. Guyon, C. Plantet, G. Agapito, C. Giordano, S. Esposito, and B. Femenia-Castella, "Adaptive optics with an infrared Pyramid wavefront sensor," in *Adaptive Optics Systems VI*, (2018).
18. C. Z. Bond, S. Cetre, S. Lilley, P. Wizinowich, D. Mawet, M. Chun, E. Wetherell, S. Jacobson, C. Lockhart, E. Warmbier, S. Ragland, C. Álvarez, O. Guyon, S. Goebel, J.-R. Delorme, N. Jovanovic, D. N. Hall, J. K. Wallace, M. Taheri, and V. Chambouleyron, "Adaptive optics with an infrared pyramid wavefront sensor at Keck," J. Astron. Telesc. Instrum. Syst. **6**(3), 039003 (2020).
19. S. Esposito, A. Puglisi, E. Pinna, G. Agapito, F. Quirós-Pacheco, J. P. Véran, and G. Herriot, "On-sky correction of non-common path aberration with the pyramid wavefront sensor," Astron. Astrophys. **636**, A88 (2020).
20. J. V. Hughes, "Sky Brightness as a Function of Altitude," Appl. Opt. **3**(10), 1135–1138 (1964).
21. L. Xu, J. Wang, K. Yao, and L. Yang, "Application of the Gaussian modeling algorithm to a Shack–Hartmann wavefront sensor for daylight adaptive optics," Opt. Lett. **46**(17), 4196–4199 (2021).
22. M. Hart, S. Jefferies, D. Hope, J. Nagy, and R. Swindle, "A Comprehensive Approach to High-Resolution Daylight Imaging for SSA," in *Advanced Maui Optical and Space Surveillance Technologies Conference (AMOS)*, (Wailea, Maui, Hawaii, USA, 2016).
23. G. M. Thomas and R. G. Cobb, "Daytime sky brightness characterization for persistent GEO SSA," in *Advanced Maui Optical and Space Surveillance Technologies Conference (AMOS)*, (Wailea, Maui, Hawaii, USA, 2017).
24. C. E. Guthery and M. Hart, "Pyramid and Shack–Hartmann hybrid wave-front sensor," Opt. Lett. **46**(5), 1045–1048 (2021).
25. O. Guyon, "Limits of Adaptive Optics for High-Contrast Imaging," Astrophys. J. **629**(1), 592–614 (2005).
26. A. Tozzi, P. Stefanini, E. Pinna, and S. Esposito, "The double pyramid wavefront sensor for LBT," in *Adaptive Optics Systems*, (2008).
27. X. Li, X. Li, and C. wang, "Improvement of correlation-based centroiding methods for point source Shack–Hartmann wavefront sensor," Opt. Commun. **411**, 187–194 (2018).
28. R. J. Noll, "Zernike polynomials and atmospheric turbulence," J. Opt. Soc. Am. **66**(3), 207–211 (1976).